Fabrication and Electrochemical Application of Three-Dimensional Gold Nanoparticles: Self-Assembly

Ahmed I. Abdelrahman, Ahmad M. Mohammad,† Takeyoshi Okajima, and Takeo Ohsaka*

Department of Electronic Chemistry, Interdisciplinary Graduate School of Science and Engineering, Tokyo Institute of Technology, Mail Box G 1-5, 4259 Nagatsuta, Midori-ku, Yokohama 226-8502, Japan

Received: October 29, 2005; In Final Form: December 23, 2005

Multilayers film of nanostructured citrate-stabilized gold particles (AuNPs) has been fabricated based on the layer-by-layer (LBL) technique using a self-assembled monolayer of 1,4-benzenedimethanethiol (BDMT). The formation of AuNPs and BDMT self-assemblies as alternative multilayers was confirmed by transmission electron microscopy (TEM), X-ray photoelectron spectroscope (XPS), and quartz crystal microbalance (QCM). The formation of uniform AuNP layers with an average monolayer thickness of 5−6 nm was obvious in the TEM images. The existence of BDMT molecules as cross linkers for the AuNPs' layers was proved by XPS measurements. The greater affinity of AuNPs' layers to bind BDMT molecules in comparison with the bare Au bulk electrode was revealed by QCM measurements. Electrochemically, the AuNPs' layers on the electrode surface did not only catalyze the reduction of oxygen (ca. 100-mV positive shift of the reduction peak potential compared with that at the bare Au bulk electrode) but also showed a fascinating nature of working as a renewed activated-electrode surface; a zigzag response was observed for oxygen reduction during alternative immobilization of BDMT and the AuNP layer. The self-assembly of a new AuNPs layer restored the catalytic activity that was entirely blocked by the preceding BDMT layer.

1. Introduction

Modification of electrode surfaces with gold nanoparticles (AuNPs) has recently received a considerable interest as a consequence of the rapid progress in nanotechnology both in fundamental studies and technological applications.[1,2] In general, and compared with their bulk materials, nanomaterials, with their size, morphology, large surface area, and possible quantum confinement, exhibit unique physical and chemical properties.[3] In particular, the dependence of the catalytic activity of metallic and metal oxide nanoclusters on the cluster size has become now a fact.[4,5] Interestingly, AuNPs exhibit an outstanding catalytic activity compared to bulk gold, which is unusual considering that bulk gold is chemically inert.[6,7] In fact, AuNPs are considered among the most stable metallic nanoparticles,[1] and they have widely been used in several aspects in chemistry,[8] material science,[9] and biotechnology.[10] In catalysis, the monolayer-protected core−shell gold/alloy nanoparticle-tailored electrodes have been used in the electrocatalytic reduction of oxygen[11] and oxidation of CO,[8] methanol,[2] and methanal.[12] To immobilize nanosized particles on a certain substrate, several approaches such as the electrodeposition and immobilization by electrostatic or covalent interactions have been sought.[13−16] Among these approaches, the layer-by-layer (LBL) self-assembly technique has been proved to be facile and flexible to generate ultrathin films with molecular order and stability.[17] In addition, the LBL method was considered as one of the best techniques for the preparation of a three-dimensional structured array of nanoparticles.[18] This technique uses natural and synthetic polyelectrolytes, biomacromolecules, and various polyionic inorganic species to fabricate multilayers. Films prepared by LBL exhibited an independent repeated electrochemical behavior for the electroactive Os^{3+}/Os^{2+} and Ru^{3+}/Ru^{2+} redox centers.[19] Olek et al.[20] have also used the LBL approach to prepare a high concentration of nanotubes with a homogeneous distribution within a polymer. Moreover, the LBL technique could be used to structure covalently linked multilayers of metallic nanoparticles on (3-aminopropyl) trimethoxysilane (APTMS)-coated glass,[21] gold,[22] and indium tin oxide (ITO) substrates using different bisthiol cross linkers.[13] These structures were useful for optical and spectroscopic applications.[23]

Recently, our group has investigated the electrochemical reduction of oxygen on AuNPs electrochemically deposited on different substrates.[24−26] These nanoparticles exhibited an extraordinary electrocatalytic activity toward oxygen reduction. We have also utilized the self-assemblies of short-chain disulfide with a terminal amino group (cystamine) and aromatic dithiol (1,4-benzenedimethanethiol (BDMT)) for anchoring AuNPs on Au substrate.[27] A significant increase in the cathodic peak current and a 130-mV positive shift in the cathodic peak potential have been observed,[27] indicating that AuNPs achieved a good electrical communication with the underlying electrode surface.

In this paper, we expand the idea to fabricate three-dimensional multilayers of AuNPs self-assembled on the surface of a gold electrode using the LBL approach and BDMT as a cross linker. The formation of covalently bonded multilayers of AuNPs and BDMT SAM over the gold electrode was examined by transmission electron microscopy (TEM), X-ray photoelectron spectroscopy (XPS), and quartz crystal microbalance (QCM) technique. Next, the electrochemical activity of AuNPs' layers and their behavior as a renewed electrode surface

* To whom correspondence should be addressed. Phone: +81-45-924-5404. Fax: +81-45-924-5489. E-mail: ohsaka@echem.titech.ac.jp.

† Permanent address: Chemistry Department, Faculty of Science, Cairo University, P. O. 12613, Giza, Egypt.

10.1021/jp056238x CCC: $33.50
Published on Web 01/21/2006

SCHEME 1: Schematic Illustration for Anchoring Colloidal Au Nanoparticles on Mercapto-Terminated Self-Assembly[a]

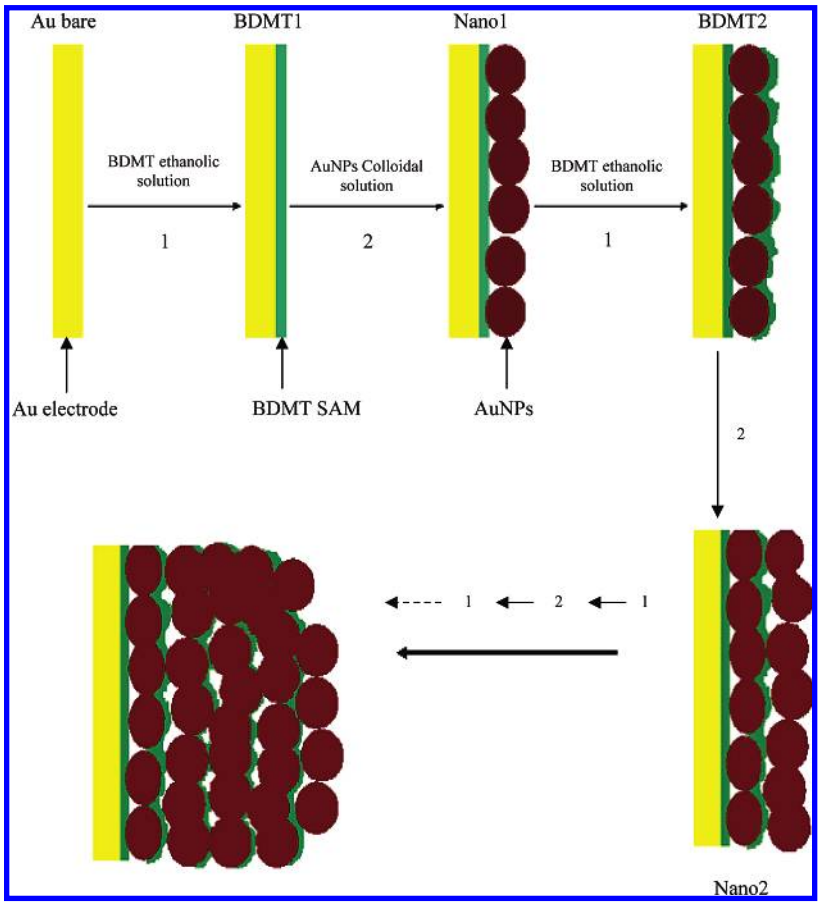

[a] Key: (1) A bare Au electrode is immersed in 1 mM BDMT ethanolic solution for 1 h, and (2) then the SAM-modified Au electrode is immersed in colloidal Au nanoparticles' solution for 12 h.

were evaluated using $[Ru(NH_3)_6]^{2+/3+}$ redox couple and oxygen reduction in neutral media.

2. Experimental Section

2.1. Fabrication of BDMT SAM and AuNPs Multilayer Modified Gold Electrodes.

All the chemicals used in this study were of analytical grade. Polycrystalline gold electrodes were used as substrates in the electrochemical, TEM, XPS, and QCM measurements in the current study. Prior to use in the electrochemical measurements, the surface of each electrode was polished with a fine emery paper and subsequently with aqueous slurries of successively fine alumina powder (down to 0.06 μm). After that, the electrodes were sonicated in Milli-Q water in an ultrasonic bath for 10 min. Next, the electrodes were cleaned electrochemically in 0.2 M H_2SO_4 by cycling the potential sweep between -0.2 and 1.5 V vs Ag|AgCl|NaCl (sat.) at a scan rate of 10 V s^{-1} for 10 min or until the cyclic voltammogram (CV) characteristic of a clean Au was obtained. However, the Au electrodes used for the TEM, XPS, and QCM measurements were only cleaned electrochemically.

The preparation and characterization of citrate-stabilized AuNPs' colloidal solution have been detailed previously.[28] Typically, 1 mL of 1% $NaAuCl_4$ was added to 90 mL of water at room temperature. After 1 min of stirring, 2 mL of 38.8 mM sodium citrate was added. Subsequently, 1 mL of freshly prepared 0.075% $NaBH_4$ in 38.8 mM sodium citrate was added and the colloidal solution was stirred for 5−10 min and stored in a dark bottle at 4 °C. The average size of Au nanoparticles in this colloidal solution was reported 2.6 nm in diameter.[28]

The BDMT SAM was prepared by soaking Au electrodes after cleaning in an ethanolic solution of 1 mM BDMT for 1 h. The as-prepared BDMT−Au electrodes were subsequently washed well with copious amount of water and ethanol and then kept in the Au colloidal solution for 12 h at room temperature. The electrodes were rinsed again with water before measurements. Hereafter the BDMT-modified Au electrodes will be referred as BDMT1 and AuNP-anchored BDMT−Au electrodes will be referred as Nano1 (see Scheme 1). BDMT molecules adsorbed on Au surface in a perpendicular orientation with loss of one thiol proton.[29] At the Nano1 electrode, the AuNPs are covalently bonded with the mercapto-terminal groups.

Fabrication of BDMT SAM and AuNP multilayers was done by repeating the above procedures (soaking in BDMT then Au colloidal solutions) times the number of layers needed. For example, to fabricate Nano4 the above procedure was repeated 4 times.

2.2. Electrochemical, TEM, XPS, and QCM Measurements.

The electrochemical measurements were performed in a two-compartment three-electrode cell with a gold working electrode (diameter 1.6 mm), a Pt wire auxiliary electrode, and a NaCl-saturated Ag|AgCl reference electrode. The redox reaction of 0.2 mM $[Ru(NH_3)_6]^{3+}$ was done in 0.1 M phosphate buffer solution (PBS) (pH 7.0). Argon gas was bubbled in the solution for 10 min prior to the measurements and allowed to flow over during the reaction. On the other hand, for the oxygen-reduction reaction, O_2 gas was bubbled for 10 min into PBS to ensure O_2 saturation and kept flowing over during the reaction. The CVs

were recorded using a computer-controlled electrochemical analyzer CHI 604A.

JEM-2010F analytical transmission electron microscope was used to capture the TEM images. The XPS spectra were recorded by ESCA3400 electron spectrometer (SHIMADZU) using an unmonochromatized X-ray source with Mg Kα (1253.6 eV) anode. For QCM measurements, an AT-cut quartz crystal was used to construct the electrochemical quartz crystal electrode as a microbalance for solution work. The crystal used had a 13-mm diameter disk for the electrochemical measurements and a 6-mm diameter disk for the microbalance measurements that oscillates in the range of 6 MHz. The quartz crystal was sandwiched between two metal electrodes bonded to the crystal surface.[30]

3. Results and Discussion

3.1. The Formation of BDMT and AuNP Multilayers.

Microscopy is undoubtedly considered among the most valuable tools for the characterization of nanoparticles, as only by direct monitoring can one obtain a precise picture of the nanoparticle size and shape. One of the most popular microscopic methods in the nanoparticles' analysis is TEM. It provides the best images, even allowing the imaging of particle crystallinity.[13]

Parts A − C of Figure 1 show the typical TEM images of Nano1, Nano2, and Nano10 mesh electrodes. One can easily estimate the layers and their average thickness, as well as the average size of AuNPs. In Figure 1A, one can almost see a uniform single layer of AuNPs with few uncovered sites on the mesh electrode surface. According to this image, the average thickness of this layer is in the range of 5−6 nm. It might be worth mentioning here that the average size of Au nanoparticles in the colloidal Au solution before immobilization on the BDMT layer was 2.6 nm.[28] Therefore, it can be anticipated that two Au nanoparticles aggregate during anchoring the AuNPs' layer. It is believed that aggregations do not occur in the citrate-stabilized Au nanoparticles solution since a negatively charged citrate sphere surrounds each particle. We expect, for these nanoparticles to be adsorbed on the BDMT layer, an instantaneous partial uncovering of the citrate spheres should take place. During this short time, two Au nanoparticles can aggregate. This assumption is supported by the fact that no more aggregations were occurred when the electrode was left in the Au nanoparticles solution for long time.

Parts B and C of Figure 1 show the TEM images for the Nano2 and Nano10 electrodes, respectively. The average thickness of layers in these images is 10−11 nm and 50−60 nm for Nano2 and Nano10, respectively. This confirms the formation of 2 and 10 layers, respectively, each of which has a thickness of ca. 5−6 nm. Therefore, the formation of successive AuNP layers could be proved from the TEM studies. Unfortunately, the TEM investigation could not show clearly the distance between two successive AuNP layers. In fact, this distance corresponds to the length of the BDMT molecule, which is very short (0.8 nm),[31] a length that is very difficult for any imaging technique to detect. However, the existence of BDMT as a cross linker for the AuNPs' layers still needs to be investigated.

To confirm that BDMT molecules are linking the Au nanoparticles layers together, XPS and QCM measurements were carried out. Selected XPS measurements are shown in Figure 2 for BDMT4 (a) and Nano4 (b) electrodes. The spectra in both cases showed a broad band in the range 160−164 eV, in agreement with a previous finding for the S2p peak.[32] Of course, two different peaks (−S−H and −S−Au) for sulfur are expected to appear. Castner et al.[32] reported that these peaks appeared at 162 and 163.5 eV for alkanethiols, i.e., within the same range we have seen for sulfur in our case. We further measured the XPS spectrum for BDMT1 layer (only one BDMT layer is adsorbed on Au substrate). In this case about 50% of −S−H and 50% of −S−Au bonds are expected to exist. However, the XPS spectrum for this sample showed again a broad band within the aforementioned range (160−164 eV).

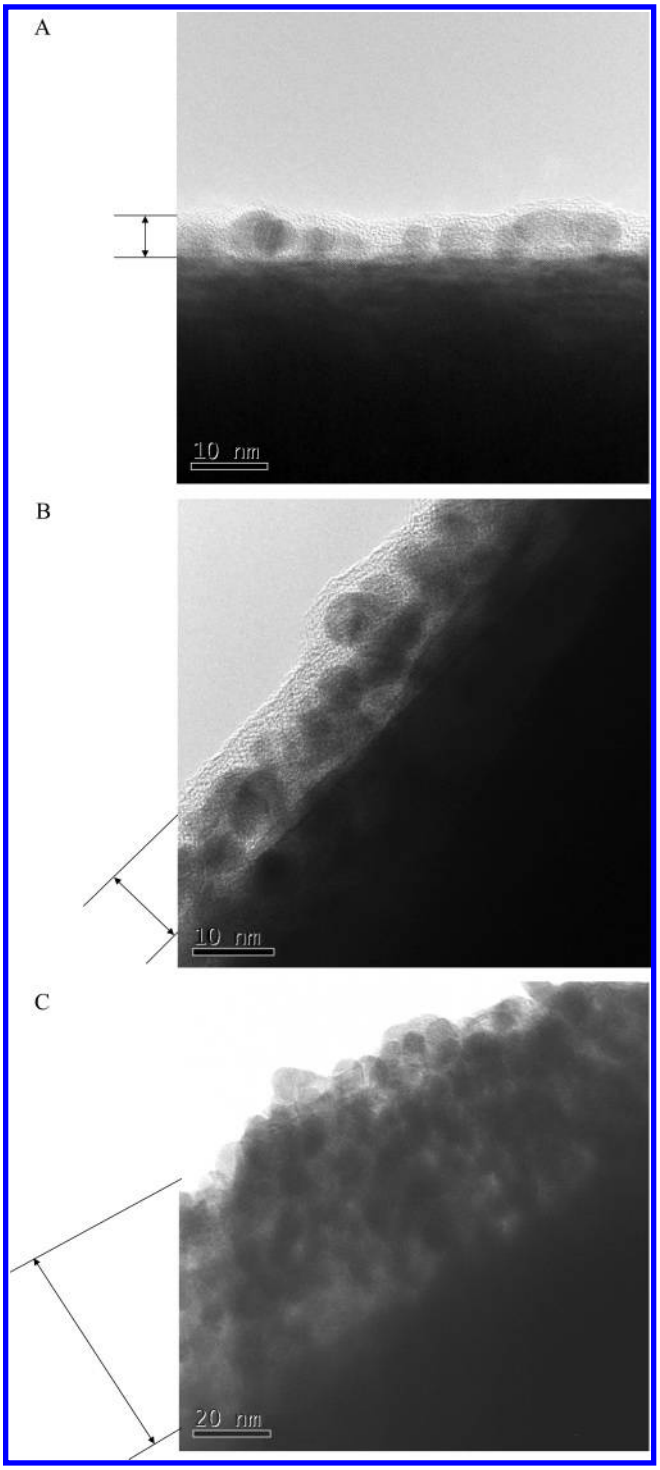

Figure 1. The TEM images for (A) Nano1, (B) Nano2, and (C) Nano10. The arrows indicate the AuNP layers. See Scheme 1 to identify the abbreviations.

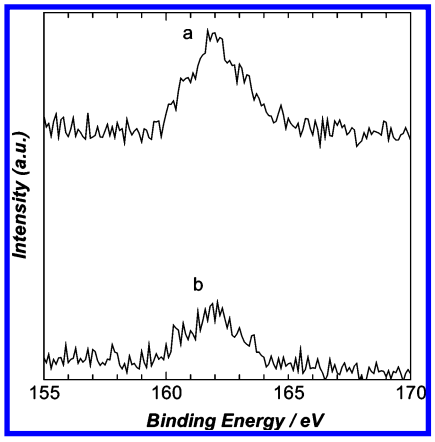

Figure 2. The XPS spectra for (a) BDMT4 and (b) Nano4. See Scheme 1 to identify the abbreviations.

This, undoubtedly, confirmed the existence of the two peaks for sulfur confined in the broad band ranged from (160−164 eV).

On the other hand, the S2p peak area of BDMT4 (Figure 2a) is relatively larger than that of Nano4 (Figure 2b), which can be attributed to the relative position of the last BDMT layer (S2p peak source). In other words, in the case of Nano4, the BDMT layer lies beneath the AuNP layer, whereas in BDMT4 the BDMT is a surface topmost layer. As well-known, XPS is a surface technique, i.e., surface topmost layers contribute more for photoemission signals than deeper layers.[33] This proves the existence of BDMT layer as a covalent cross linker between the AuNPs layers.

QCM measurements revealed some more details about these BDMT and AuNP self-assembled multilayers. The amount of AuNPs anchored in the first layer was lower than that immobilized in the next layers (the frequency change, $\Delta f = 238.7$ Hz for Nano1 and ca. 300 Hz for the other layers), which is in agreement with the TEM investigation. As shown previously, some uncovered or defected spots appeared in the TEM images for Nano1 (Figure 1A) and disappeared in the next layers (parts B and C of Figure 1). This can be attributed to the existence of some surface imperfections or defects in the Au substrate. These imperfections led to the incomplete coverage of BDMT in the first layer, and consequently, the amount of BDMT assembled in the first layer was less than that assembled in the other layers ($\Delta f = 11.7$ Hz for BDMT1 and ca. 21.5 Hz for the other layers). The ratio (1.8) of the amount of BDMT assembled in the second and further layers to that in the first layer is much higher than the ratio (1.3) of the amount of AuNPs anchored in the second and further layers to that in the first layer. The higher amount of BDMT assembled, in the second and higher layers, is due to larger surface area of AuNPs in comparison to the bare Au bulk electrode.

3.2. Electrochemical Results.

CV measurements of redox markers such as the $[Ru(NH_3)_6]^{2+/3+}$ couple were performed to probe the nature of monolayer-modified electrodes. Investigation whether the electron transfer occurred through tunneling over the BDMT barrier or directly through the defected sites in the barrier was also aimed. Figure 3 shows the CVs obtained at bare polycrystalline Au, BDMT1, Nano1, Nano2, and Nano10 electrodes for the $[Ru(NH_3)_6]^{2+/3+}$ redox couple in neutral solution. A well-defined reversible voltammogram characteristic of a diffusion-controlled redox process was observed at the bare polycrystalline Au electrode (Figure 3a). A quasireversible voltammogram was observed at BDMT1 electrode for the $[Ru(NH_3)_6]^{2+/3+}$ couple.

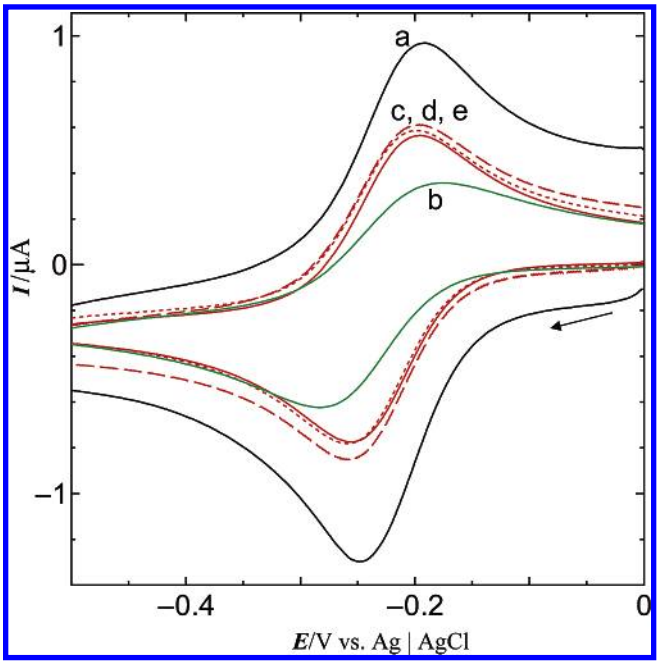

Figure 3. CVs obtained for the redox reaction of 0.2 mM $[Ru(NH_3)_6]^{3+}$ at (a) bare, (b) BDMT1, (c, dotted line) Nano1, (d, solid line) Nano2, and (e, dashed line) Nano10 electrodes in 0.1 M Ar-saturated phosphate buffer solution (pH 7.0). Potential scan rate: 100 mV s^{-1}.

Compared to the bare electrode, an obvious increase in the ΔE_p value (110 mV) and a significant decrease in the peak current have been noticed (Figure 3b) for BDMT1, implying that the rate of electron transfer at this electrode is slow. We believe that the hydrophobic nature and the compactness of BDMT monolayer are hindering the permeation of the redox molecules. However, as can be seen from Figure 3c, an increase in the peak current along with a decrease in the ΔE_p (60 mV) has further been noticed at the Nano1 electrode. Nano2 and Nano3 behaved similarly to Nano1 (parts d and e of Figure 3). The standard electron-transfer rate constant (k_s) for the redox reaction of the $[Ru(NH_3)_6]^{2+/3+}$ couple was calculated using the Nicholson theory.[34] The modification of surface of a gold electrode by the self-assembly of BDMT decreases the k_s value by a factor of 50 ($k_s^{bare} = 5.0 \times 10^{-1}$ cm s^{-1}; $k_s^{BDMT} = 1.0 \times 10^{-2}$ cm s^{-1}). The k_s value at the Nano1 electrode is very similar to that at the bare Au electrode. It revealed that the Au nanoparticles on the BDMT monolayer acted as a new electrode surface and that the particles on the electrode surface achieved a good electrical communication with the underlying electrode surface through the monolayer.[27,14] The electrical conduction through BDMT using an electrochemically deposited platinum electrode has recently be detailed by Campbell et al.[31] This can be supported from the potential-step chronoamperometric measurements for the reduction of $[Ru(NH_3)_6]^{3+}$ at bare, BDMT1, Nano1, Nano2, and Nano10 electrodes in 0.1 M phosphate buffer solution. That is, the Cottrell slope obtained at the bare electrode was 0.66 μA $s^{1/2}$, which is larger than that obtained at the BDMT1 electrode (0.46 μA $s^{1/2}$). Whereas, after immobilization of Au nanoparticles, the Cottrell slope obtained at the Nano1 electrode was found to increase significantly (0.82 μA $s^{1/2}$). Assembling of the second BDMT layer decreased the Cottrell slope to 0.68 μA $s^{1/2}$, which in turn increased again to 0.88 μA $s^{1/2}$ after anchoring the AuNP second layer. Thus, the effective surface area of the AuNP-modified electrodes (Nano1, Nano2) was larger than that of the bare Au- and BDMT-modified electrodes (BDMT1, BDMT2). Table 1 summarizes a comparison between the different modified electrodes in the

TABLE 1: Electrochemical Data for $[Ru(NH_3)_6]^{3+}$ Redox Reaction and O_2 Reduction at Various Gold Electrodes in 0.1 M Phosphate Buffer Solution (pH 7.0)

	$[Ru(NH_3)_6]^{2+/3+}$ redox reaction			O_2 reduction	
electrodes	ΔE_p[a] mV	Cottrell slope[b] μA s$^{1/2}$	k_s[c] cm s^{-1}	E_{pc}[d] V vs Ag|AgCl	I_{pc}[d] μA
bare	60	0.66	5.0×10^{-1}	−0.22	10.0
BDMT1	110	0.46	1.0×10^{-2}		
Nano1	60	0.82	5.0×10^{-1}	−0.12	11.5
Nano2	59	0.88		−0.12	11.4
Nano10	61	0.86		−0.12	11.7

[a] Data were obtained from Figure 3 at a scan rate of 100 mV s^{-1}. [b] Data were obtained from potential step chronoamperometric measurements at various electrodes for the reduction of 0.2 mM $[Ru(NH_3)_6]3+$ in 0.1 M phosphate buffer solution (pH 7.0). [c] Data were obtained from ref 25 at a scan rate of 150 mV s^{-1}. [d] Data were obtained from Figure 4 at a scan rate of 100 mV s^{-1}.

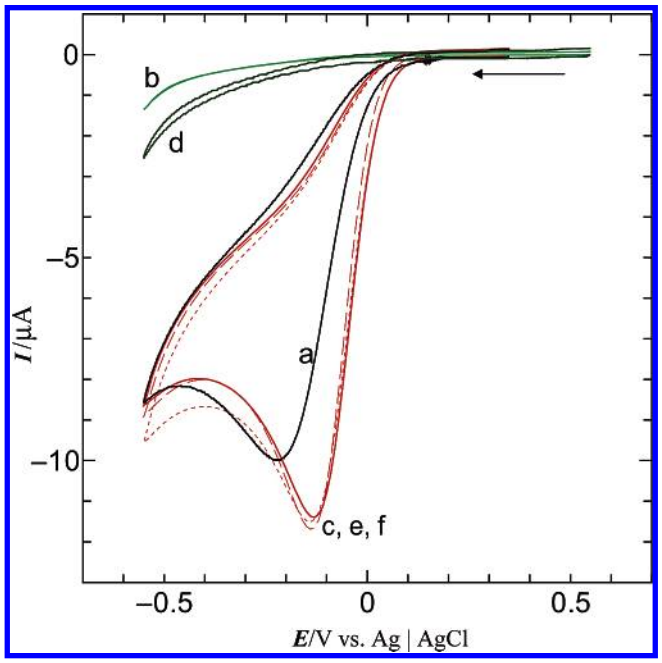

Figure 4. CVs obtained for the oxygen reduction at (a) bare, (b) BDMT1, (c, dotted line) Nano1, (d) BDMT2, (e, solid line) Nano2, and (f, dashed line) Nano10 electrodes in 0.1 M O_2-saturated phosphate buffer solution (pH 7.0). Potential scan rate: 100 mV s^{-1}.

potential peak separation ΔE_p, Cottrell slope, and standard rate constant calculated by Nicholson approach for the reduction of 0.2 mM $[Ru(NH_3)_6]^{3+}$.

We have also examined the electrocatalytic activity of the AuNP layers toward the reduction of oxygen. Figure 4 represents the CVs obtained for the reduction of oxygen at the bare, BDMT1, Nano1, BDMT2, Nano2, and Nano10 electrodes. The two-electron reduction of oxygen to hydrogen peroxide at the polycrystalline Au electrode occurred at around −0.22 V (Figure 4a), while the BDMT1 electrode did not show any voltammetric response for the reduction of oxygen in the potential range used in this investigation (Figure 4b). Indeed, the self-assembled monolayer (SAM) on the electrode surface is expected to kinetically impedes the electron transfer between the electrode surface and the electroactive species in solution.[25] Surprisingly, that happened only for the oxygen reduction reaction over the BDMT monolayer. Neither $[Ru(NH_3)_6]^{2+/3+}$ nor $Fe^{2+/3+}$ redox couples experienced this hindrance.[27] We suppose that the hydrophobic nature and compactness of the BDMT monolayer and/or the shortage of $H^+(H_3O^+)$ near the BDMT monolayer are behind this unusual behavior of oxygen reduction on BDMT1. Proceedings of the reaction through either an inner sphere or outer sphere mechanism may also contribute. It is believed that the outer-sphere mechanism is open to all redox active systems, while the inner-sphere mechanism, which is likely the mechanism for oxygen reduction, requires substitution-labile reactants and products. This issue needs further investigation and is under our focus now.

At the Nano1 electrode, a well-defined wave for the reduction of oxygen was observed at −0.12 V, which is 100 mV less negative than that at the polycrystalline Au electrode, implying that the immobilized Au nanoparticles efficiently catalyze the reduction of oxygen. The sharp cathodic peak associated with an enhancement in the peak current reflects a fast electron transfer at the Nano1 electrode. The reduction process was proved to be diffusion controlled at the nanoparticle-immobilized electrode, as evidenced by the linear increase of peak current with the square root of potential scan rate.[27] Interestingly, there was no response for the reduction of oxygen, after assembling the second BDMT layer (Figure 4d). The second AuNP layer restored the catalytic activity toward the oxygen reduction (Figure 4e). This behavior (losing the catalytic activity for oxygen reduction on BDMT monolayers and restoring it over AuNPs monolayers) has repeated for all the next layers as a zigzag response up to 20 alternative layers of BDMT and AuNP (10 layers for each). It is interesting that the response for the oxygen reduction is completely suppressed when BDMT is assembled as a topmost layer, while a renewed-catalyzed response is obtained at the AuNPs' modifies electrode (see Figure 4f for Nano10 and Table 1 for the cathodic peak potential (E_{pc}) and current (I_{pc}) for different electrodes.

Our results in this paper confirmed strongly the good electrical communication of the AuNPs with the underlying electrode surface and further proved the electrocatalytic behavior of AuNPs. In addition, serving the alternative AuNP layers as a renewed activated-electrode surface is a new finding that will definitely open the doors for further applications in the electrochemical catalysis. Furthermore, our fabrication scheme for the three-dimensional AuNP self-assembled film with the smooth electron transfer and controlled layer thickness can be utilized in the molecular devices development.

4. Conclusions

The fabrication of AuNP multilayers has been demonstrated using BDMT SAMs. TEM images proved the formation of repeatedly uniformed AuNP layers with an average monolayer thickness of 5−6 nm. The existence of BDMT as a cross linker between the AuNP layers was also verified.

The AuNP layers immobilized on mercapto-terminated self-assemblies of BDMT achieved good electrical communication with the underlying electrode surface and, further, worked as a renewed activated-electrode surface. These AuNP layers showed a good electrocatalytic activity toward oxygen reduction (100 mV positive shift) and efficiently restored the catalytic activity that was entirely inhibited by the preceding BDMT layer. Further work is needed to understand the nature of the electron transfer

through the layers, and the effect of different substrates (like single crystalline surfaces) on the structural quality and length of the films.

Acknowledgment. The present work was financially supported by Grant-in-Aids for Scientific Research on Priority Areas (No.417), Scientific Research (No. 12875164), and Scientific Research (A) (No. 10305064) to T. Ohsaka, from the Ministry of Education, Culture, Sports, Science and Technology, Japan (Monbu-kagakusho) and also by New Energy and Industrial Technology Development Organization, Japan. The authors acknowledge Dr. A. Genski and Professor K. Suga at TIT for their assistance in the TEM and XPS measurements, respectively. They also thank Dr. M. S. El-Deab for his helpful discussions regarding the experimental results. A.I.A. acknowledges a Monbu-kagakusho scholarship from the Japanese Government.

References and Notes

(1) Daniel, M.-C.; Astruc, D. *Chem. Rev.* **2004**, *104*, 293−346 and the references therein.
(2) Zhong, C.-J.; Maye, M. M. *Adv. Mater.* **2001**, *13*, 1507−1511.
(3) Alivisatos, A. P. *Science* **1996**, *271*, 933−937.
(4) Henry, C. R. *Appl. Surf. Sci.* **2000**, *164*, 252.
(5) Tsodikov, M. V.; Rostovshchikova, T. N.; Smirnov, V. V.; Kiseleva, O. I.; Maksimov, Y. V.; Suzdalev, I. P.; Ikorskii, V. N. *Catal. Today* **2005**, *105*, 634.
(6) (a) Biswas, P. C.; Nodasaka, Y.; Enyo, M.; Haruta, M. *J. Electroanal. Chem.* **1995**, *381*, 167−177. (b) Maye, M.; Lou, Y.; Zhong, C.-J. *Langmuir* **2000**, *16*, 7520−7523.
(7) Zhou, H.; Dong, S. *Guijinshu* **2004**, *25*, 48−56.
(8) (a) Cliffel, D. E.; Hicks, J. F.; Templeton, A. C.; Murray, R. W. In *Metal Nanoparticles*; Feldheim, D. L., Foss, C. A., Eds.; Marcel Dekker: New York, 2002; pp 297−317. (b) Haruta, M. *Catal. Today* **1997**, *37*, 153−166. (c) Bethell, D.; Brust, M.; Schiffrin, D. J.; Kiely, C. *J. Electroanal. Chem.* **1996**, *409*, 137−143.
(9) (a) Fendler, J. H.; Meldrum, F. C. *Adv. Mater.* **1995**, *7*, 607−632. (b) Schmid, G. *Chem. Rev.* **1992**, *92*, 1709−1727.
(10) (a) Mirkin, C. A.; Letsinger, R. L.; Mucic, R. C.; Storhoff, J. J. *Nature* **1996**, *382*, 607−609. (b) Elghanian, R.; Storhoff, J. J.; Mucic, R. C.; Letsinger, R. L.; Mirkin, C. A. *Science* **1997**, *277*, 1078−1081. (c) Alivisatos, A. P.; Johnsson, K. P.; Peng, X.; Wislon, T. E.; Loweth, C. J.; Bruchez, M. P., Jr.; Schultz, P. G. *Nature* **1996**, *382*, 609−611. (e) Dong, S.; Tang, C. *Guijinshu* **2005**, *26*, 53−61.
(11) Wang, B. *J. Power Sources* **2005**, in press.
(12) Stelmach, J.; Hotze, R.; Brzeinska, M. B.; *J. Electroanal. Chem.* **1994**, *377*, 241−247.
(13) Shipway, A.; Katz, N. E.; Willner, I. *Chem. Phys. Chem.* **2000**, *1*, 18−52 and the references therein.
(14) Sagara, T.; Kato, N.; Nakashima, N. *J. Phys. Chem. B* **2002**, *106*, 1205−1212.
(15) Freeman, R. G.; Grabar, K. C.; Allison, K. J.; Bright, R. M.; Davis, A. J.; Guthrie, A. P.; Hommer, M. B.; Jackson, M. A.; Smith, P. C.; Walter, D. G.; Natan, M. J. *Science* **1995**, *267*, 1629−1635.
(16) Chan, E. W. L.; Yu, L. *Langmuir* **2002**, *18*, 311−313.
(17) Decher, G. *Science* **1997**, *277*, 1232−1237.
(18) (a) Hicks, J. F.; Young, S.-S.; Murray, R. W. *Langmuir* **2002**, *18*, 2288−2294. (b) Feldheim, D. L.; Grabar, K. C.; Natan, M. J.; Mallouk, T. E. *J. Am. Chem. Soc.* **1996**, *118*, 7640−7641. (c) Hu, X.; Cheng, W.; Wang, T.; Wang, Y.; Wang, E.; Dong, S. *J. Phys. Chem. B* **2005**, *109*, 19385−19389.
(19) Yang, M.; Yang, Y.; Yang, H.; Shen, G.; Yu, R. *Biomaterials* **2006**, *27*, 246−255.
(20) Olek, M.; Ostrander, J.; Jurga, S.; Mohwald, H.; Kotov, N.; Kempa, K.; Giersig, M. *Nano Lett.* **2004**, *4*, 1889−1895.
(21) Musick, M. D.; Keating, C. D.; Keefe, M. H.; Natan, M. J. *Chem. Mater.* **1997**, *9*, 1499−1501.
(22) Brust, M.; Etchenique, R.; Calvo, E. J.; Gordillo, G. J. *Chem. Commun.* **1996**, *16*, 1949−1950.
(23) Baum, T.; Bethell, D.; Brust, M.; Schiffrin, D. J. *Langmuir* **1999**, *15*, 866−871.
(24) El-Deab, M. S.; Ohsaka, T. *Electrochem. Commun.* **2002**, *4*, 288−292.
(25) El-Deab, M. S.; Okajima, T.; Ohsaka, T. *J. Electrochm. Soc.* **2003**, *150*, A851-A857.
(26) El-Deab, M. S.; Sotomura, T.; Ohsaka, T.; *Electrochem. Commun.* **2005**, *7*, 29−34.
(27) Raj, C. R.; Abdelrahman, A. I.; Ohsaka, T. *Electrochem. Commun.* **2005**, *7*, 888−893.
(28) Brown, K. R.; Walter, D. G.; Natan, M. J. *Chem. Mater.* **2000**, *12*, 306−313.
(29) Murty, K. V. G. K.; Venkataramanan, M.; Pradeep, T. *Langmuir* **1998**, *14*, 5446−5456.
(30) Oyama, N.; Ohsaka, T. *Prog. Polym. Sci.* **1995**, *20*, 761−818.
(31) Kim, B.; Ahn, S. J.; Park, J. G.; Lee, S. H.; Park, Y. W.; Campbell, E. E. B. *Thin Solid Films*. In Press.
(32) Castner, D. G.; Hinds, K.; Grainger, W. *Langmuir* **1996**, *12*, 5083−5086.
(33) (a) Ertl, G.; Küppers, J. *Low Energy Electrons and Surface Chemistry*; VCH Verlagsgesellschaft: Weinheim, 1985. (b) Lopez-Salido, I.; Lim, D. C.; Kim, Y. D. *Surf. Sci.* **2005**, *588*, 6−18.
(34) Bard, A. J.; Faulkner; L. R. *Electrochemical Methods Fundmentals and applications*; Wiley: New York, 2001; Chapter 6.